T1
86

NAVAL RESEARCH

REVIEWS

OCTOBER 1974

RECEIVED
DEC 31 1974
NAVAL POSTGRADUATE SCHOOL LIBRARY

F -IENCE

Philip H. DuBois

Philip H. DuBois is Professor Emeritus of Psychology at Washington University, St. Louis, Missouri. He is renowned for his work in psychological statistics and testing. One of his many publications, "An Introduction to Psychological Statistics," is an important text in the field.

For many years Professor DuBois directed an ONR project pertaining to the problems of technical training. This work led to the development and application of multiple part correlation as a way of describing the learning process. Another book "Multivariate Correlational Analysis" was based on this work.

In 1973 Professor DuBois chaired an ONR panel that made recommendations on appropriate statistical methods for handling data considered in making promotions of Navy enlisted men.

Grinding Damage in Ceramics

B. G. Koepke and R. J. Stokes

Honeywell Corporate Research Center
Bloomington, Minn.

Introduction

For many modern applications ceramics must be machined to high tolerances requiring a grinding, lapping, polishing sequence. Extremely high stresses and temperatures are generated at the tool workpiece interface. These stresses promote plastic flow and/or cracking depending on the machining parameters and the mechanical properties of the ceramic workpiece. As a result the finished surface contains dislocations, cracks and residual stress. These defects can have a major impact on the particular application of a ceramic. It is of paramount importance to understand this influence of defects on the physical properties of ceramics and to learn corrective measures that can be employed so that ceramics can achieve their full potential in components, devices and systems.

Ceramic materials are finding increased application in modern technology because of the wide range of physical properties they offer. For example, the chemical stability, high modulus and hardness of alumina and boron carbide make them ideal materials for components in gas bearing gyroscopes where dimensional stability and wear resistance are needed. The combination of good magnetic properties, low electrical conductivity and high hardness make ferrites suitable for high frequency recording heads. Ceramics are also used for their special piezo-electric, magneto-optic, electro-optic and ferroelectric properties in modern devices.

In many of these applications the ceramic components are either very tiny or must be fabricated to high tolerances (microinches) often with surfaces flat within the wavelength of light. This kind of precision is beyond the capability of primary fabrication techniques whether they be slip casting, sintering, hot pressing or crystal growth. As a result, secondary fabrication is an essential step in the manufacturing process, and the art of machining ceramics by grinding, lapping

---

*Dr. Koepke and Dr. Stokes are Senior Research Scientist and Manager, respectively, in the Materials Science Department, Honeywell Inc. Corporate Research Center. Their main fields of interest are deformation and fracture and the effects of microstructure on the physical properties of ceramics.

and polishing is now very advanced. While considerable attention has been given to the development of polishing techniques, cutting tools and abrasives, comparatively little attention has been given to the state of the surface of the ceramic material so produced. Recognizing the lack of available information concerning this important aspect of ceramic machining, the Office of Naval Research has supported a number of projects in this area for the past five years. This activity has been concerned with both detailed characterizations of the states of ceramic surfaces before and after abrasive machining and with understanding the interaction between tool and workpiece during the machining process itself. This paper reviews some of this activity, particularly the knowledge gained on the nature and consequence of grinding damage.

Mechanical Response of Ceramics

It is important to realize at the outset that ceramics are not the completely hard, brittle materials normally supposed. Indeed all ceramics can undergo some plastic deformation.* The ease and extent to which ceramics are deformable is dependent on their atomic bond strength, crystal structure and chemical composition. One way of distinguishing the response of ceramics to mechanical stress is indicated by the classification in Table 1.

Table 1 can only be used as a rough guide to the mechanical response expected of a ceramic during grinding since this classification applies for typical uniaxial tensile tests at strain rates of 10^{-3} sec^{-1} and for homogeneously heated samples. The states of stress, strain rate and temperature at the tool workpiece interface as a chip is cut are extreme and vary with grinding wheel type, depth of cut, feed rate and thermal conductivity of the ceramic. The strain rate under ordinary grinding conditions approaches 10^{7} sec^{-1}. The temperatures at which a chip is cut can also be high. In a series of elegant experiments supported by the Naval Bureau of Weapons, P. Gielisse and J. Stanislao at the University of Rhode Island have measured directly temperatures of 1500°C at the chip while grinding ceramics with a single diamond point mounted on a high speed wheel. Using the single point diamond wheel, these researchers have shown that under certain

*Plastic deformation refers to the *permanent* change in shape induced in a sample when a load is applied and removed. It is important to realize that the amount of plastic deformation generally observed in ceramics is much less than that found in metals. Furthermore plastic deformation in ceramics is very localized as for example in the immediate vicinity of a hardness indentation. Even the so-called "ductile" ceramics do not deform on the scale found in most metals.

TABLE 1
Mechanical Behavior of Ceramics

Category	Deformation Conditions	Examples
Completely Brittle	Hard – Dislocations Cannot Move Until Stresses Approach Theoretical Strength Brittle – Noncrystallographic Crack Propagation (Conchoidal Fracture)	Alumina Boron Carbide Silicon Carbide Barium Titanate
Semi-Brittle	Soft – Dislocations Can Move at High Stresses Brittle – Crystallographic Crack Propagation (Cleavage Fracture)	Magnesia Ferrite
Ductile	Soft – Dislocations Can Move at Low Stresses Over Many Crystalline Planes	Silver Chloride Sodium Chloride at 300°C

circumstances the grinding operation may be regarded as a series of extremely high temperature, high strain rate impacts. When the cutting efficiency of the single diamond point drops, grinding becomes a high temperature, high strain rate smearing operation.

Clearly the mechanical behavior of a ceramic is important in its response to a machining operation, but of greater importance are the machining conditions, namely wheel type, rate of material removal and stress state at the chip.

Nature of Grinding Damage in Single Crystals

In this section we will describe the damage introduced into ceramic single crystals by a simple semi-rough grinding operation in which

typically one mil of material is removed in a single pass under a grinding wheel rotating at 3000 r.p.m. The direction of rotation of the wheel is such that it bites into a workpiece as shown in Figure 1 – generally referred to as "climb grinding" (experience shows that "climb grinding" is the only way to machine many ceramics without shattering). We will distinguish between the actual state of the surface (surface damage) and the situation in the material immediately beneath the surface (subsurface damage).

For a start, let us consider grinding a single crystal slice of magnesium oxide. Here we find a great difference in the damage, depending on whether the diamond or the aluminum wheel is used. Diamond wheels have "closed" structures, (i.e. the abrasive grains protrude from a continuous matrix) and do not load readily when grinding magnesia. Alumina wheels on the other hand generally have "open" structures, (i.e. the wheel structure is porous and the binder is not continuous) Figure 2. If a diamond wheel is used the multiple impacts of the abrasive grains protruding from the wheel matrix cause the

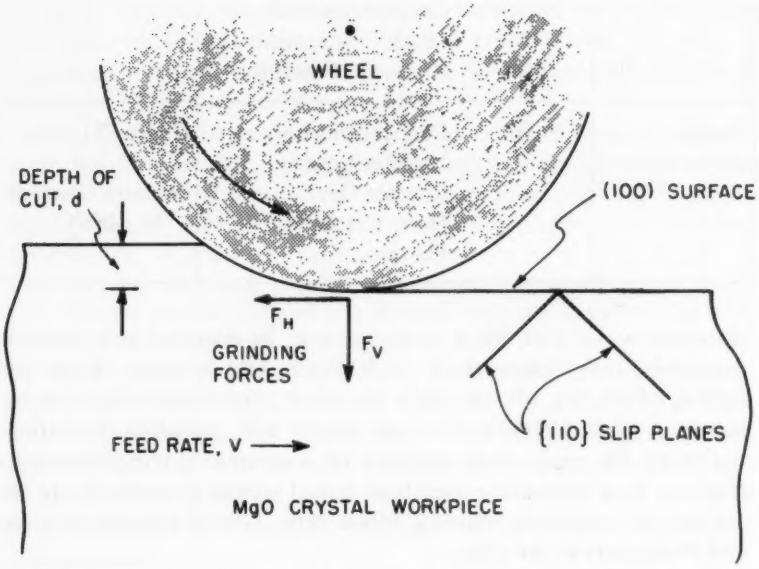

Figure 1 – Schematic showing the wheel-workpiece geometry during a climb-grinding pass on a magnesium oxide crystal workpiece. The cutting face of the wheel moves in the same direction as the workpiece. In the orientation shown, the workpiece is least liable to fracture since slip on {110} planes at 45° to F_V relieves the grinding stresses.

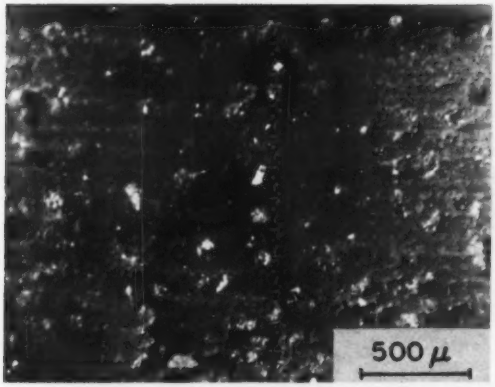

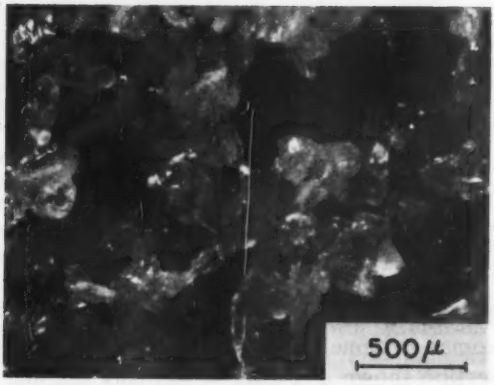

Figure 2 – Photomicrographs of the cutting faces of two types of grinding wheels. The diamond wheel has a "closed" structure in the sense that the abrasive grains protrude from a continuous matrix of binder. The alumina wheel, on the other hand, has an "open" structure with a cutting face that contains a large number of voids.

surface of the crystal to be chipped away through a series of {100}* cleavage fractures. When the crystal is oriented so that the {100} planes make an angle to the machined surface the cleavage cracks then propagate beneath that surface to produce the extremely rough cross section illustrated in Figure 3. If an alumina wheel is used to grind magnesium oxide, the pores fill with swarf, the material removal mechanism becomes extremely inefficient and the surface heats up.

*The {100} planes in a cubic crystal are those planes that lie perpendicular to the three principal axes of the cubic unit cell. i.e. the faces of the cube. Brittle fracture in MgO occurs generally by cleavage on these cube planes.

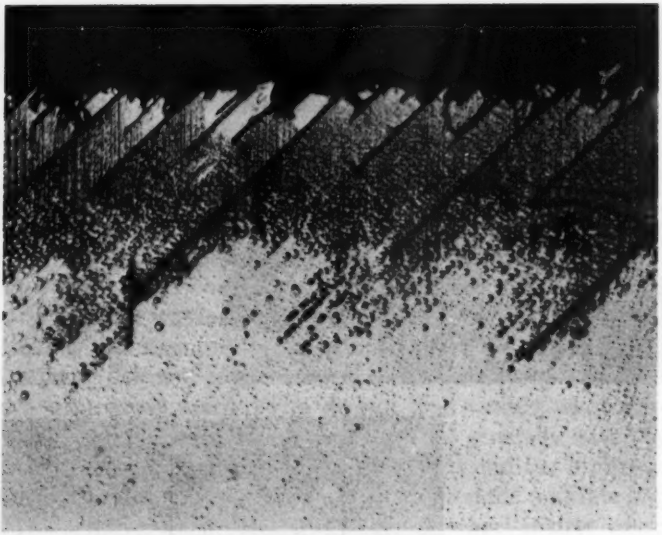

Figure 3 – {100} cross section through a magnesium oxide crystal ground with a 100 grit diamond wheel. The machined surface (top) was {110}. Grinding has introduced a large number of subsurface {100} cleavage cracks. The cracks extend to the bottom of a highly deformed layer as revealed by dislocation etch pits. Magnification 250X.

The rise in temperature promotes plastic flow and the surface becomes extremely smooth and burnished as illustrated by the cross section shown in Figure 4. Actually thermal quenching causes a fine network of thermal cracks to be produced in the otherwise smooth surface.

Magnesium oxide single crystals have the distinct advantage that they can be cleaved and the cross section etched to reveal dislocation activity beneath the ground surface. The dense layers of etch pits visible in Figures 3 and 4 immediately beneath the ground surface clearly show there is always a layer of intense slip and a high density of residual dislocations left by the machining operation. R. Rice, at the Naval Research Laboratory, has made similar observations. When machining is performed with a diamond wheel the plastically deformed layer is uneven in extent reflecting the impact nature of its introduction; when the surface is burnished with an alumina wheel, the layer is very even and precisely defined. This latter observation prompted a series of experiments in which depth of the damage layer was correlated with changes in the machining variables associated with rate of material removal and orientation of the single

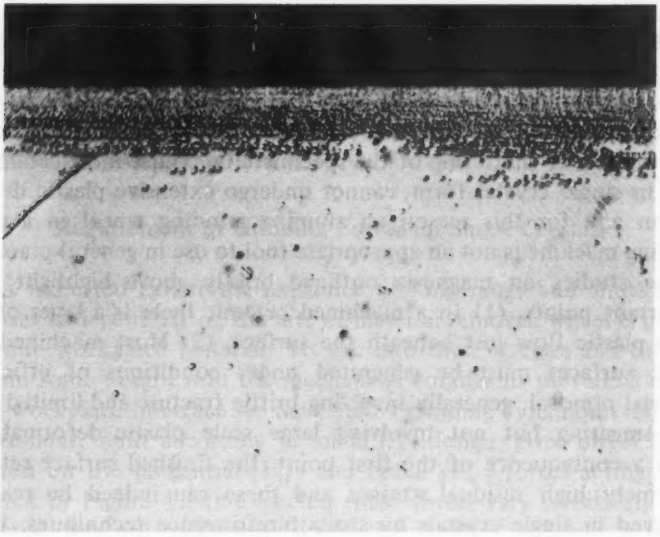

Figure 4 – {100} cross section through a magnesium oxide crystal ground with a 46 grit alumina wheel. The machined surface (top) was {100} (i.e. – same configuration as Fig. 1). Grinding has introduced a uniform, plastically deformed layer as revealed by dislocation etch pits. Magnification 250X.

crystal. It was found that as the rate of material removal was raised the depth of the plastically deformed layer increased, extending as deep as 200μm. Furthermore, it was found that material removal by plastic flow was only possible so long as the crystal was favorably oriented for shear under the mechanical stresses imposed by the alumina grinding wheel. In the $\{100\}$ surface orientation shown in Figure 1, two $\{110\}$* slip surfaces are equally and favorably oriented at 45°. Crystals ground with the alumina wheel in other orientations shattered.

The above observations may be understood by distinguishing the effects of short range and long range grinding stresses on the work-piece (the crystal). Immediately adjacent to the wheel the stress gradients are extremely steep as attested by the discrete nature of the slipped layer. These short range stresses originate from the high thermal gradients and mechanical stresses at the cutting points. Long

*The {110} planes in a cubic crystal are those planes lying at 45° to two of the principal axes of the unit cell and parallel to the other one, i.e. diagonal planes. Plastic deformation in MgO occurs generally by shear across these diagonal planes.

range stresses originate when the workpiece is forced between the wheel and the machine bed as can be appreciated from Figure 1. So long as the swarf is cleared (as with the diamond wheel) the long range stresses do not build up; but if the swarf is not cleared, long range compressive stresses arise which can only be relaxed by plastic deformation or shattering of the specimen. Of course most ceramics, even in single crystal form, cannot undergo extensive plastic deformation and for this reason an alumina grinding wheel in a rigid grinding machine is not an appropriate tool to use in general practice.

The studies on magnesia outlined briefly above highlight two important points; (1) In a machined ceramic there is a layer of intense plastic flow just beneath the surface, (2) Most machined ceramic surfaces must be generated under conditions of efficient material removal, generally involving brittle fracture and limited surface smearing but not involving large scale plastic deformation.

As a consequence of the first point, the finished surface retains extremely high residual stresses, and these can indeed be readily observed in single crystals by stress birefringence techniques. With special care the optical retardation can be measured and the residual stress determined from the stress optic coefficient. We have shown that a residual compressive stress extends to the depth of the plastically deformed layer reaching a magnitude corresponding to a significant fraction of the yield strength of the crystal. This stress field must naturally be balanced by a residual tensile stress extending much deeper into the material.

The observations made on surface plastic flow in magnesium oxide single crystals have been repeated on other ceramic materials. The extent of the deformation and the resolution of the dislocations is dependent on the material and the means of detection. For example in sapphire the dislocation layer is extremely shallow ($<1\mu$) and can be studied adequately only by transmission electron microscopy as has been shown by B. Hockey at the National Bureau of Standards, in his Office of Naval Research sponsored work. Becher at the Naval Research Laboratory, has extended these observations using etch pit techniques. Discrete dislocation layers introduced in other hard ceramic materials by machining have also been observed by transmission electron microscopy in some instances and by effects due to residual stresses and stress birefringence in others.

The important point to note here is that *all* ceramic materials which have been machined by abrasive techniques contain residual surface dislocations extending to a depth varying from 1μ to 200μ depending on the overall hardness of the material and the severity of the machining operation. In addition, of course, there will be

subsurface cracking of the kind illustrated in Figure 3 depending on the orientation of cleavage planes and the particular machining conditions. These two features of the machined ceramic, subsurface dislocations and cracking, have a profound influence on their physical properties as we shall outline in a later section.

Measurement of Grinding Forces on Single Crystals

As indicated earlier the existence of long range and short range stresses is dependent on the rate of material removal, wheel type and ceramic workpiece material. To measure these stresses and thereby obtain some insight into the mechanical conditions prevailing at the tool-workpiece interface we have used a grinding dynamometer. This instrument, built according to an M.I.T. design, gives direct information on the tangential (F_H) and radial (F_V) forces acting as indicated in Figure 1. As expected these forces vary sensitively with material removal rate and, when the surface is being removed largely by plastic flow, with the orientation of single crystals.

The important point about measuring grinding forces is that it is possible following the analysis due to M. Shaw, to derive the specific grinding energy ($\bar{U}$).

$$\bar{U} = \frac{\pi nD}{Vdb} F_H \qquad (1)$$

where n = wheel speed, D = wheel diameter, V = workpiece feed rate, d = wheel depth of cut, b = width of cut. This corresponds to the work done per unit volume of material removed. $\bar{U}$ has the dimensions of stress and interestingly enough, through extensive argument, can be shown to be equal to the stress at the chip involved in chip removal. Our measurements on magnesia single crystals give values for $\bar{U}$ approaching the theoretical shear strength, indicating the magnitude of the stress at the chip to be also of this order of magnitude. In light of this result, it is not surprising that observations of plastically deformed layers on machined ceramic surfaces are turning out to be the rule rather than the exception.

The grinding force dynamometer has also been applied to another interesting aspect of surface machining namely the enhancement of material removal by certain liquid environments. Westwood at Advanced Institute for Scientific Research (AISR), in work sponsored by the Office of Naval Research, has shown remarkable effects of the environment (i.e. matching fluid) on drilling rates in ceramics. The dependence is sensitive to the conditions of material removal,

whether by the plastic flow or brittle fracture. While our complementary measurements of the effects of environment on grinding forces did not show a straightforward correlation with Westwood's drilling data, variations with environment were noted.

Nature of Grinding Damage in Polycrystals

Polycrystals may only be machined with diamond tools. As we have noted earlier two major types of grinding damage occur in diamond machined ceramic single crystals, a subsurface zone of plastic deformation and cracked surfaces generated by fracture (conchoidal or cleavage). As might be expected the same features exist in polycrystals, but in addition surface cracking occurs due to intergranular separation. Grain boundary fracture is the source of "pull out", a feature common to all ground polycrystalline ceramic workpieces.

Actually it is our experience that the softer, weaker semi-brittle ceramics demonstrate very extensive intergranular separation as illustrated in Figure 5. In the hard, completely brittle ceramics, regions

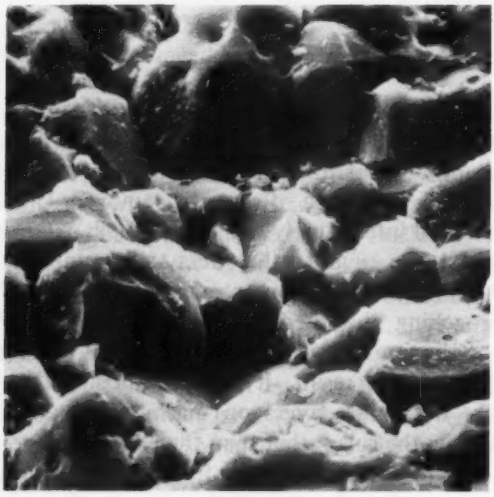

Figure 5 – Scanning electron micrograph of sintered polycrystalline Ni-Zn ferrite ground with a 100 grit diamond wheel. In a ceramic with low impact resistance, material removal occurs mainly by brittle intergranular fracture. Grinding direction – horizontal.

of intergranular fracture are found but there are also extensive surface regions generated by plastic flow or burnishing as shown in Figure 6. This is not surprising when we recall first, from the dynamometer measurements, that the stresses under each abrasive grain approach the theoretical strength and second, from the observations of Gielisse and Stanislao that the temperatures can be quite high. Furthermore the impact strengths (particularly with respect to intergranular fracture) of many completely brittle ceramic polycrystals exceed those of the softer semibrittle ceramics. Thus extensive surface plastic flow is expected to occur during machining. In fact it is our observation that the hardest polycrystalline ceramics such as boron carbide show the most extensive burnishing during semirough machining.

The depth of damage introduced into a polycrystalline ceramic during any particular machining step is an important quantity for reasons to be discussed later. At this time few quantitative studies have been made of this aspect of machining and questions pertaining to the nature and extent of the damage in polycrystalline ceramics remain unanswered.

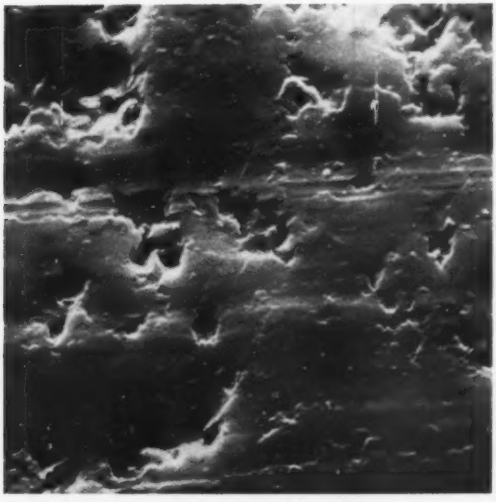

Figure 6 – Scanning electron micrograph of hot pressed polycrystalline alumina ground with a 100 grit diamond wheel. In a ceramic with high impact resistance, material removal occurs mainly by plastic flow. Grinding direction horizontal. Magnification 2000X.

Measurement of Grinding Forces on Polycrystals

We have mentioned that measurements of grinding forces with the dynamometer can be used to derive the specific grinding energy for a given machining configuration. This parameter has been determined for a number of different polycrystalline ceramics and some representative values are listed in Table 2.

TABLE 2

Specific Grinding Energy, U, for Different Polycrystalline Ceramics

Material	$U(10^{10}\,erg/cm^2)$	U/G	$E\gamma\left(10^{12}\,\frac{erg^2}{cm^5}\right)$
Magnesia (MgO)	26	.2	3
Spinel ($MgAl_2O_4$)	30	.3	–
Lucalox (Al_2O_3)	75	.5	11
Avco Hot Pressed Alumina (Al_2O_3)	200	1.2	–
Coors AD999 Alumina (Al_2O_3)	110	.7	14
Boron Carbide (B_4C)	190	1	21

Specimens all ground with a 100 grit diamond wheel at a moderate rate of material removal. G, shear modulus; $E\gamma$ fracture toughness parameter. E, Young's modulus; γ, effective surface energy.

As the middle column shows, the value for U is a significant fraction of the shear modulus illustrating the point mentioned earlier that the stresses on a chip are on the order of the theoretical shear strength (G/10) of crystalline materials. The right hand column indicates there is a reasonable correlation also between the specific grinding energy and the fracture toughness parameter $E\gamma$. This is expected since, as mentioned above, the amount of surface plastic flow should increase as the fracture resistance of the workpiece increases.

From these observations and measurements it is possible to make some general comments concerning the nature of the grinding process in polycrystalline ceramics.

- The stress on a chip is high and can approach the theoretical shear strength.
- The surface layer contains a high dislocation density.
- In weak polycrystalline ceramic materials the impact of the cutting points causes material to separate intergranularly.
- In tough polycrystalline ceramic materials the cutting points remove more material by plastic flow causing severe temperature gradients.
- Thermal quenching can cause cracking or spalling of the surface after the wheel has gone by.
- Measurements of specific grinding energy show some correlation with the fracture toughness for different ceramics indicating an increasing contribution of plastic flow during material removal from tougher ceramics.

Physical Consequences of Grinding Damage

As a result of the above nature of the grinding process it must be realized that the ground surface of a ceramic has certain features associated with it, namely;

- Surface dislocations
- Residual stress
- Surface cracks

These three basic features have an influence on the physical properties of a ceramic. The feature which is dominant depends on the particular physical property of interest.

If we are using a ceramic for its *mechanical properties* then surface cracking is particularly important. Brittle fracture is well known to originate from surface flaws, the critical fracture stress σ_f is related to the surface crack dimension, C, through the Griffith equation;

$$\sigma_f = \sqrt{\frac{E\gamma}{C}}$$

Obviously enhancement of the mechanical strength will follow if special care is taken to prepare a surface free from cracks. This can be achieved with sequential fabrication steps of decreasing severity, that is, hogging to rough grinding to fine grinding to polishing and lapping, providing each successive step *completely* removes the full extent of the damage due to the former. This latter point is one which is often completely overlooked in ceramic machining because plastic flow

can smear a ceramic surface to hide earlier defects and give the impression they have been eliminated.

The extent of residual damage was made clear to us in an experience with gas bearing gyroscopes fabricated out of fine grained alumina. For this application mating gas bearing surfaces are finished to microinch tolerances with running gaps of a few microinches. The gaps are so narrow that the pull out of a single grain at a corner can jam the bearing. To generate gas pressure between the bearing surfaces, aerodynamic grooves are machined into the surfaces. It has been common practice to machine these grooves by grit blasting them into the finished ceramic surfaces after the final lapping operation. Unfortunately this relatively rough operation not only caused cracking of the material at the base of the grooves; it also exposed subsurface cracks introduced by the prior machining. In addition grit blasting introduced surface stresses which reinforced the centrifugal stresses to cause grains of material to 'pop out' of the surface during operation and jam the bearing causing costly failures. The resolution to this problem was first to execute extreme care during the sequence of machining operations to make sure that all previous damage had been removed down to the finished dimension and second to machine the grooves by a nonmechanical, such as ion beam machining, method. The resulting grooves were crack and stress free and the expulsion of debris was eliminated. Solution to this troublesome problem was based on the experience gained from fundamental studies of machining mechanisms and surface condition.

If we are using a ceramic for its *magnetic properties* then residual stresses and the stress fields associated with the surface dislocations are particularly important. The contribution of stress is through the magnetostriction coefficient and its influence on permeability and domain mobility. Domain boundaries become hung up along lines of defects remaining from machining operations as illustrated dramatically in Figure 7. In this case magnetic bubble domains in epitaxial magnetic garnet layer are held up by residual stresses imparted from the underlying garnet which had been mechanically lapped. To overcome this problem obviously the substrates had to be carefully lapped, polished and stress relieved.

The effects of residual stress on the permeability of a nickel-zinc ferrite is equally dramatic. Figure 8 shows B-H loops of a torroidal sample of ferrite before and after annealing. A decrease in permeability induced by grinding can be restored by annealing and vice versa. This degradation of magnetic properties in machined ferrites has been found to depend on the sample size becoming more pronounced as the specimen (toroid) thickness decreases. The reason

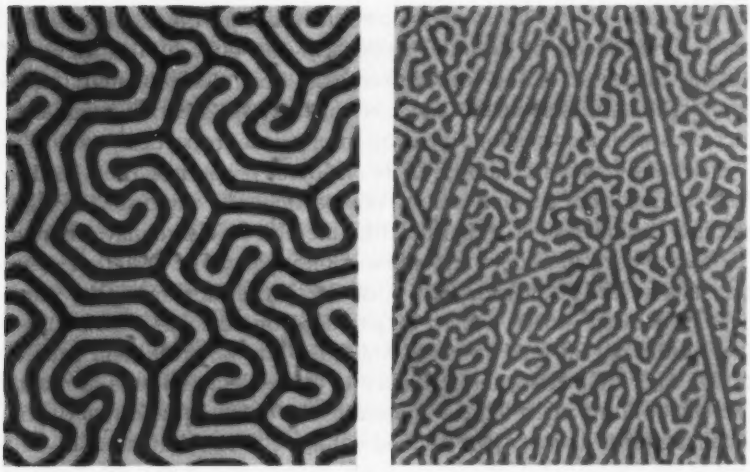

(a) (b)

Figure 7 – Effect of substrate surface preparation on magnetic domain configuration in an epitaxial garnet layer. In (a) the domain boundaries are clearly held up along residual scratches. In (b) the substrate is carefully lapped, polished and stress relieved to produce equilibrium domain configuration. Magnification 160X. (Courtesy T. S. Liu and R. B. Fryer, Honeywell Corporate Research Center.)

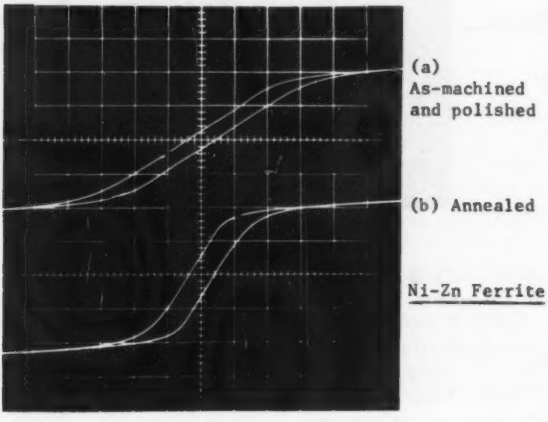

Figure 8 – Effect of surface condition on the B-H loop of a Ni-Zn ferrite toroid showing degradation of magnetic properties resulting from ceramic machining (Courtesy J. R. Kench, Honeywell Corporate Research Center.)

for this lies in the layer of stressed material at the surface which must be balanced by residual stresses in the bulk of the material. As the thickness of the toroid decreases, the volume of material to support the stress decreases and consequently the internal stress level increases with a corresponding drop in physical properties.

If we are using a ceramic for its *electrical properties* then surface dislocations and surface cracks are particularly important. Piezoelectric ceramics such as barium titanate and lead zirconate-titanate (PZT) are used in underwater sonar applications. The design of sonar transducers for good signal to noise resolution demands that internally generated 'noise' due to localized corona discharge be reduced to a minimum. Surface flaws are well known to be prominent sources of the high field strengths necessary to cause electrical breakdown of the surrounding air. Figure 9 illustrates the detrimental effect of this localized breakdown on the applied voltage-current characteristic of a

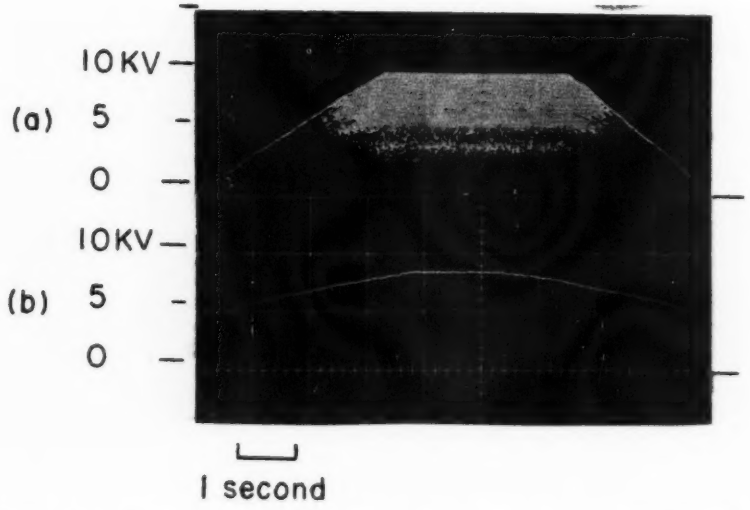

Figure 9 – Effect of surface flaws on the incidence of corona discharge in a PZT sonar transducer ring. CRT display records many positive half cycle voltage traces (60 Hz; a.c.). Image intensity enhancement at voltage maxima gives trace of applied voltage. Image intensity enhancement when charge flow exceeds 5 picocoulombs indicates when corona discharge takes place. (See R. G. Johnson and S. J. Tibbetts, Rev. Sci. Inst. **44**, *519 (1973)).*

(a) Shows incidence of corona discharge above 5 KV in a surface defective PZT ceramic.

(b) Shows no corona discharge as voltage is raised to 10 KV. (Courtesy R. G. Johnson, Honeywell Corporate Research Center.)

for this lies in the layer of stressed material at the surface which must be balanced by residual stresses in the bulk of the material. As the thickness of the toroid decreases, the volume of material to support the stress decreases and consequently the internal stress level increases with a corresponding drop in physical properties.

If we are using a ceramic for its *electrical properties* then surface dislocations and surface cracks are particularly important. Piezoelectric ceramics such as barium titanate and lead zirconate-titanate (PZT) are used in underwater sonar applications. The design of sonar transducers for good signal to noise resolution demands that internally generated 'noise' due to localized corona discharge be reduced to a minimum. Surface flaws are well known to be prominent sources of the high field strengths necessary to cause electrical breakdown of the surrounding air. Figure 9 illustrates the detrimental effect of this localized breakdown on the applied voltage-current characteristic of a

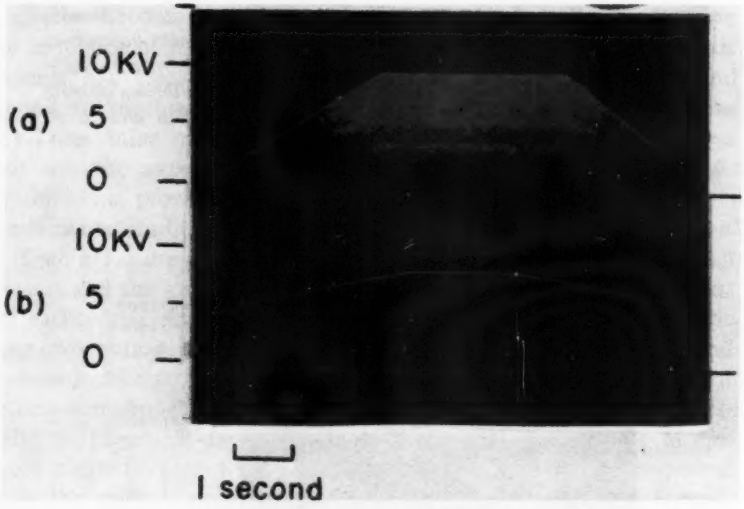

Figure 9 – Effect of surface flaws on the incidence of corona discharge in a PZT sonar transducer ring. CRT display records many positive half cycle voltage traces (60 Hz; a.c.). Image intensity enhancement at voltage maxima gives trace of applied voltage. Image intensity enhancement when charge flow exceeds 5 picocoulombs indicates when corona discharge takes place. (See R. G. Johnson and S. J. Tibbetts, Rev. Sci. Inst. **44**, *519 (1973)).*

(a) Shows incidence of corona discharge above 5 KV in a surface defective PZT ceramic.

(b) Shows no corona discharge as voltage is raised to 10 KV. (Courtesy R. G. Johnson, Honeywell Corporate Research Center.)

PZT type ceramic transducer. Elimination of flaws by careful fabrication procedures to produce smooth crack free surfaces greatly minimizes the incidence of corona discharges and permits use of the transducers at higher voltages thus exploiting the full capability of the material.

If we are using a ceramic for its *optical properties* then surface cracks and residual stresses are particularly important. The scattering of light due to surface defects has obvious effects on the transmission and reflection of optical windows and mirrors. Residual stresses in the surface can cause stress birefringence in otherwise optically inactive materials. This results in polarization and scattering of the light. In many special applications of optical ceramics such as in high energy infrared laser windows and transparent piezoelectric ceramics for displays, the slight changes in optical behavior due to residual stresses induced by polishing can be ruinous. In these cases it is essential to insure the components are stress free, either by post-fabrication annealing treatments or by chemical polishing.

Bibliography

Ceramic Processing, Publication 1576, National Academy of Sciences, Washington, D.C. (1968).

The Science of Ceramic Machining and Surface Finishing, edited by S. J. Schneider Jr. and R. W. Rice, National Bureau of Standards (U.S.) Special Publication No. 348 (1972).

NRL Innovates Unique Optically Pumped Collision Laser

– Scientists at the Naval Research Laboratory (NRL) have designed and successfully tested a continuous wave (cw) laser on the 546.1 nanometer (nm) line of Mercury (Hg I) by optically pumping a mixture of nitrogen (N_2) and Hg vapor.

Nicholas Djeu, a research physicist in the Laboratory's Optical Sciences Division and the program's principal investigator, reports that the NRL laser is based on a novel concept which combines optical pumping of the upper laser level with the collisional quenching of the lower laser level using nitrogen. And, Djeu says, the new laser should attain at least 0.1 percent efficiency in the visible green region.

In the NRL experiment, optical pumping of the laser medium is obtained from a 20-Mhz electrodeless lamp coaxial with the laser tube. The laser tube itself is 3 mm in diameter and has an active length of 30 cm. The laser has the capability to convert approximately one half the light absorbed at 404.7 nm to a laser output of 546.1 nm.

A Subsurface Light Data Sphere for Irradiance Measurements

C. Neefus and G. C. McLeod

New England Aquarium
Boston

The measurement of irradiance in the upper layers of the ocean is important in evaluating the photosynthetic activity of marine phytoplankton. The photosynthetic activity of marine phytoplankton is not only important in the food chain but knowledge of phytoplankton population characteristics is important for communication and detection systems design and operation. Unfortunately, systematic and complete spectral measurements of irradiance in coastal and oceanic environmentals are lacking. The scarcity of light data applicable to photosynthesis studies results from the technical difficulties of constructing a sensitive spectroradiometer with an omnidirectional sensor. Such a detector must be capable of resolving narrow wavelength bands in the visible spectrum. The resulting irradiance measurement obtained is the light environment of phytoplankton. The subsurface light data sphere (SLDS) discussed here is an advance in the solution of this problem of measurement of selective attenuation of irradiance. This sphere was developed under an office of Naval Research contract.

Instrumentation

The subsurface light data sphere has been designed to measure variations in spectral irradiance incident on a point receptor in the water column. Since photosynthesis is a function of a pigment system, the spectral separation of the light field is accomplished by a method capable of resolving molecular absorption bands. The narrow angle radiance collector scans the light field in a vertical plane. Scanning several known vertical planes allows the extrapolation of all directional components of irradiation about a point. The directional components can be integrated to obtain a total spectral irradiance value,

---

*Dr. Neefus is Research Associate at the New England Aquarium. Biological Oceanography is his main field of research.

Dr. McCloud is Director of Research at the New England Aquarium specializing in environmental and pollution studies of coastal waters.

or they may be kept distinct to analyze the geometric distribution of flux. The spectral sensitivity of the instrument is radiometrically flat and the output is linear and capable of spanning nine orders of magnitude of incident radiation. The instrument has been calibrated in radiometric units as opposed to photometric units which are applicable only to human vision. The field applicability of the instrument requires ruggedness, portability, and the ability to withstand water pressures at the lower limits of the photic zone.

The instrument is housed in a 13-inch pressure-tested glass sphere. Light enters through a 2-inch wide longitudinal band which is continuously scanned by a narrow angle collector. The collected light is separated into its visible spectral components via a rotating continuous variable interference filter. The transmitted light is received by a Varian 9664B photomultiplier tube (Figure 1) and the amplified signal is summed with two internally generated reference square waves which locate the beginning and end of each spectral scan.

The output of the SLDS is an analogue voltage signal. Figure 2 is a photograph of an oscilloscope display of the signal. Wavelength varies linearly along the temporal (x) axis while the corresponding

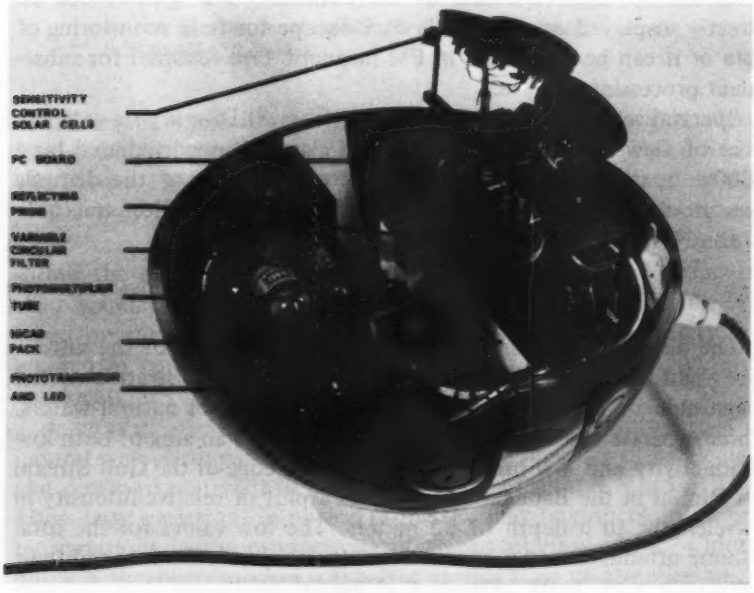

Figure 1 – Subsurface light data sphere.

or they may be kept distinct to analyze the geometric distribution of flux. The spectral sensitivity of the instrument is radiometrically flat and the output is linear and capable of spanning nine orders of magnitude of incident radiation. The instrument has been calibrated in radiometric units as opposed to photometric units which are applicable only to human vision. The field applicability of the instrument requires ruggedness, portability, and the ability to withstand water pressures at the lower limits of the photic zone.

The instrument is housed in a 13-inch pressure-tested glass sphere. Light enters through a 2-inch wide longitudinal band which is continuously scanned by a narrow angle collector. The collected light is separated into its visible spectral components via a rotating continuous variable interference filter. The transmitted light is received by a Varian 9664B photomultiplier tube (Figure 1) and the amplified signal is summed with two internally generated reference square waves which locate the beginning and end of each spectral scan.

The output of the SLDS is an analogue voltage signal. Figure 2 is a photograph of an oscilloscope display of the signal. Wavelength varies linearly along the temporal (x) axis while the corresponding

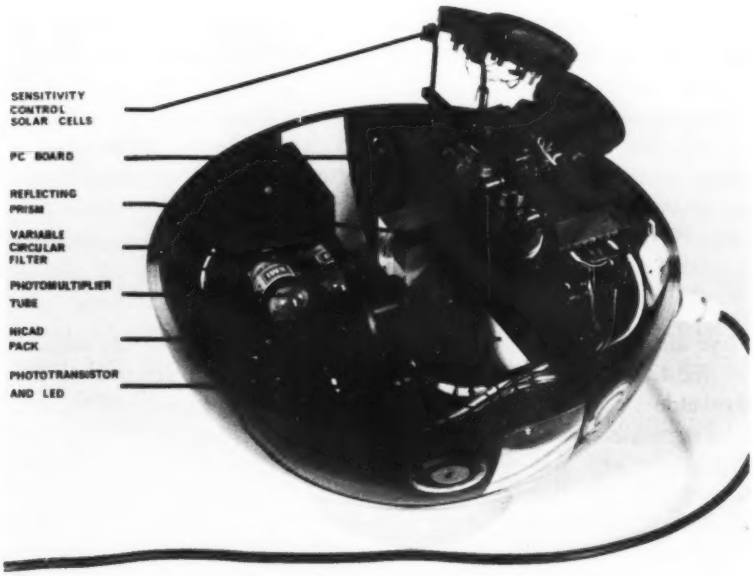

Figure 1 – Subsurface light data sphere.

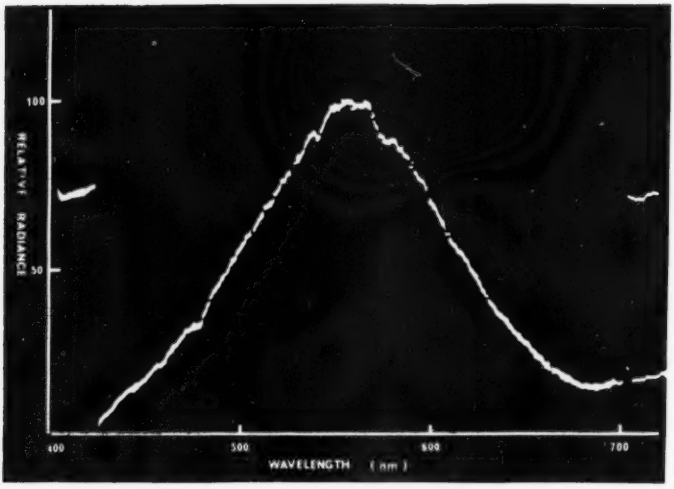

Figure 2 – Oscilloscope display of the output signal during a single spectral scan of the SLDS. Triggering and reference pulses are located at 400 nm and 700 nm.

voltage (y value) is proportional to the spectral radiance within the instantaneous field of view of the collector. The output can be directly displayed on a portable oscilloscope for field monitoring of data or it can be stored by an FM magnetic tape recorder for subsequent processing and use.

Spectral sensitivities were calculated from SLDS outputs with the field of view entirely filled by an opal glass diffuser irradiated by a 1000w quartz iodine lamp. The spectral radiance of the diffuser was measured by a spectroradiometer with a calibration traceable to the National Bureau of Standards.

Data and Results

The data described are from preliminary field tests of the subsurface light data sphere, and are included here as illustrative of the magnitude of the variability of optical properties of natural waters. Three separate cases will be discussed. The first is an area of both low productivity and low turbidity found on the edge of the Gulf Stream off Bimini in the Bahamas. Figure 3 is a plot of relative intensity in wavelengths to a depth of 60 meters. The low values for the total volume attenuation and irradiance attenuation coefficients and their constancy with depth indicate that Bimini waters are clear and uniform. The low values along with the knowledge that the wavelength

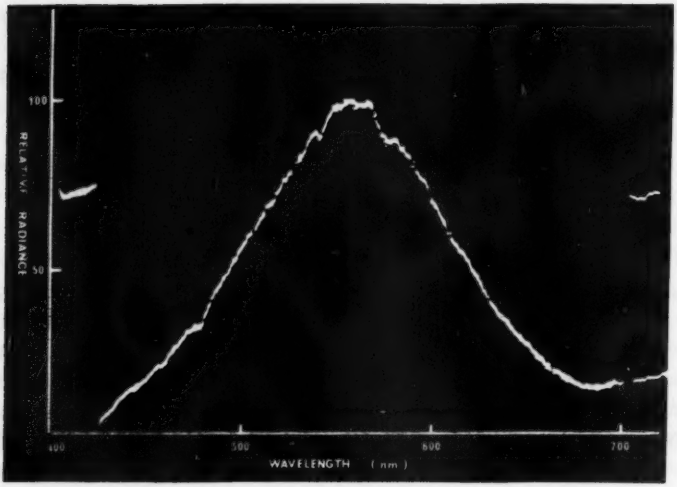

Figure 2 – Oscilloscope display of the output signal during a single spectral scan of the SLDS. Triggering and reference pulses are located at 400 nm and 700 nm.

voltage (y value) is proportional to the spectral radiance within the instantaneous field of view of the collector. The output can be directly displayed on a portable oscilloscope for field monitoring of data or it can be stored by an FM magnetic tape recorder for subsequent processing and use.

Spectral sensitivities were calculated from SLDS outputs with the field of view entirely filled by an opal glass diffuser irradiated by a 1000w quartz iodine lamp. The spectral radiance of the diffuser was measured by a spectroradiometer with a calibration traceable to the National Bureau of Standards.

Data and Results

The data described are from preliminary field tests of the subsurface light data sphere, and are included here as illustrative of the magnitude of the variability of optical properties of natural waters. Three separate cases will be discussed. The first is an area of both low productivity and low turbidity found on the edge of the Gulf Stream off Bimini in the Bahamas. Figure 3 is a plot of relative intensity in wavelengths to a depth of 60 meters. The low values for the total volume attenuation and irradiance attenuation coefficients and their constancy with depth indicate that Bimini waters are clear and uniform. The low values along with the knowledge that the wavelength

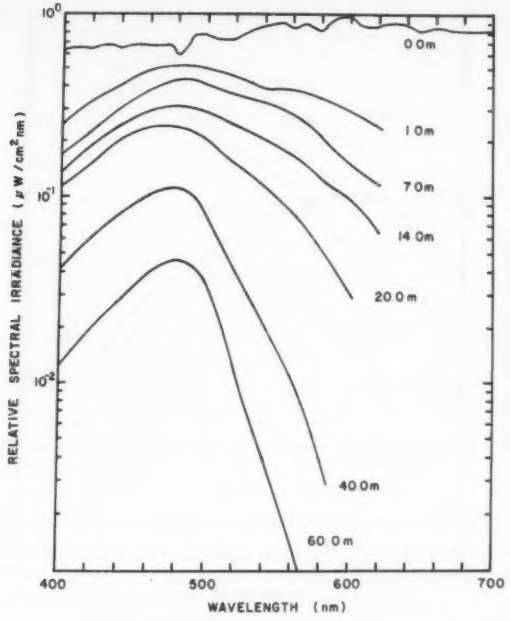

Figure 3 – Relative spectral irradiance for a series of depths in the Gulf Stream 5 miles west of Bimini, Bahamas.

of maximum transmittance lies within the 480-495 nm range places Bimini waters into the clear natural water classification (Tyler, Smith and Wilson, 1972).

The only diurnal or seasonal variations of spectral distribution in clear ocean water is attributed to changes in sun angle. Figure 4 shows the spectral distribution of light just below the surface in clear water off Bimini. The variation over time is quite small. It is based on these data that spectral variation in incident radiation is ignored in comparing submarine spectral data from different times and locations.

A number of studies have shown that the optical properties of natural waters are particularly sensitive to the presence of particulate and dissolved materials in the water column (Taylor & Smith, 1970). Thus, large variations in optical properties may be principally caused by variations in the productivity of marine phytoplankton. Chlorophyll is the main substance involved in this type of attenuation. In an area of moderate chlorophyll concentration and low non-photosynthetic turbidity, such as Woods Hole Harbor and Massachusetts

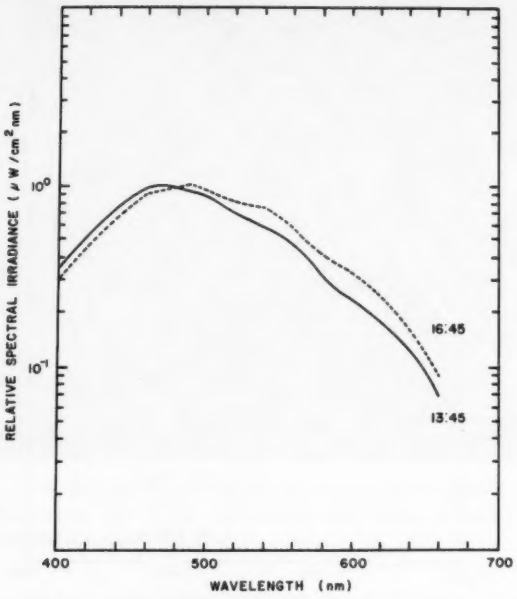

Figure 4 – Variation in spectral distribution of irradiance from 13:45 EST to 16:45 EST. These data were taken 1.0 m below the surface of the water off Bimini.

Bay, the spectral distribution of submarine light will be determined by the composite attenuations of chlorophyll, auxiliary pigments, the water, and scattering from the chlorophyll containing organisms. Although the proportions of these effects will vary, the spectrum will be dominated by the water plus chlorophyll in the upper layers. Chlorophyll is limited to the upper layers of the water column and is often stratified. Strata can be seen in the light data as step-like changes in attenuation coefficient with depth. At the lower depth limit of the pigment containing organisms, the attenuation coefficients for all wavelengths will resume the value for clear ocean water. Figure 5 demonstrates the variation in attenuation through the phytoplankton layer. It can be seen that at about 20 meters the slope becomes quite constant. The attenuation coefficient below this depth remains at a value which is close to the attenuation coefficient of clear water at the same wavelength measured in Bimini.

With the shift to moderately productive areas there is also a shift in the wavelength of maximum transmittance from 480-495 nm to nearer 550 nm (Figure 6) in waters of Woods Hole and Boston

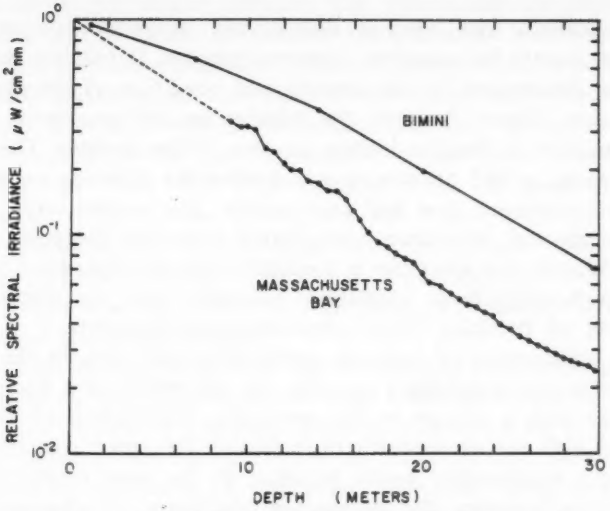

Figure 5 – Irradiance vs. depth at 530 nm at a point in Massachusetts Bay 20 miles off-shore from Boston (Aug. 22). There is a noticeable step-like attenuation due to stratified phytoplankton in the upper layers.

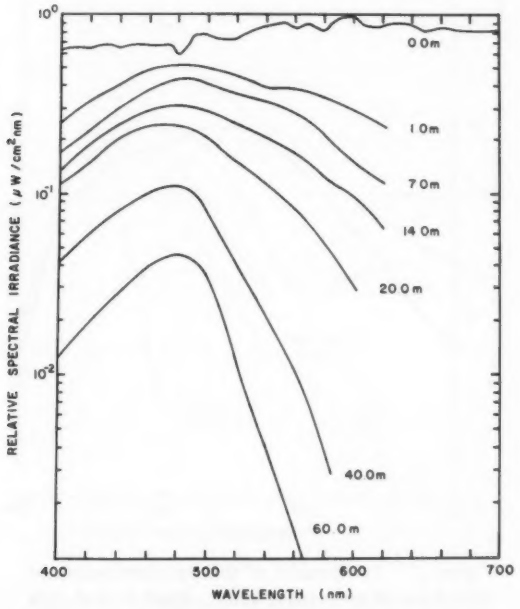

Figure 6 – The variation with depth of the spectral irradiance in Boston Harbor (May 24).

Outer Harbor. The spectral distribution in productive areas is affected greatly by plankton pigment systems. It exhibits seasonal variance determined by the density and condition of the plankton population. Figure 7 shows the relative spectral irradiance at the same location in Boston Harbor on two different dates. The curve which peaks at 565 nm was measured when the plankton population was at its summer low and fairly stable. The second curve is the relative spectral irradiance immediately following the peak of the spring bloom; the spectrum is dominated by the absorption spectra of non-photosynthetic predatory plankton and the degradation products of breaking down phytoplankton pigments.

The attenuation of light by particulate scattering in the water column is non-wavelength specific. Its net effect is a decrease in intensity and a change in the geometric distribution of flux. In areas of high non-photosynthetic turbidity, the spectral distribution vs. depth relationship would be close to the same relationship in clear water; however, the attenuation coefficients of all wavelengths

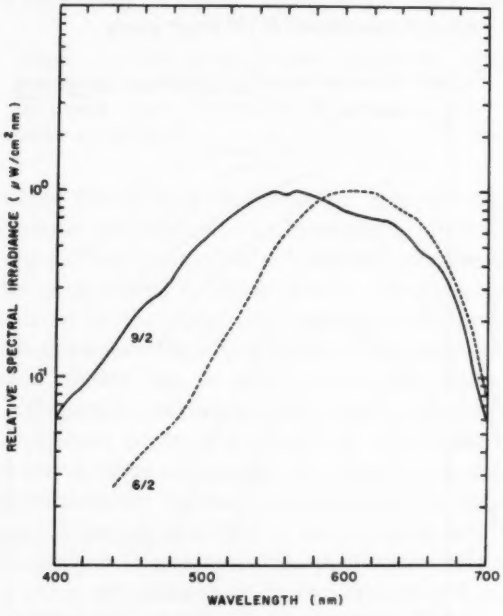

Figure 7 – Comparions of spectral distribution on two days three months apart. Both sets of data were taken at the same location in Boston Inner Harbor at a depth of 3 m.

would be proportionally greater. The attenuation by particulate scattering can therefore be assessed using a single wavelength. By choosing a non-absorbing wavelength of chlorophyll, the effects of particulate scattering can be evaluated even in productive waters with minimum interference from molecular absorption. The attenuation will be essentially the sum attenuation of the water column and scattering. In areas with high concentrations of photosynthetic organisms, the particulate attenuation will reflect the stratification of the plankton due to scattering from the surface and internal structures of the organisms. Particulate attenuation profiled against depth is shown in Figure 8 for a wide range of conditions in Boston Harbor and Massachusetts Bay.

Although the measurement of subsurface light conditions specifies the radiant energy available for photosynthesis, the degree of utilization of the energy by phytoplankton is determined by a dynamic interrelationship between variables of the light environment, chemical and physical properties of the water, including temperature and nutrient levels, the plankton population, and photosynthetic rate (Steele, 1962). The usefulness of subsurface light data is dependent on the accurate definition of this relationship.

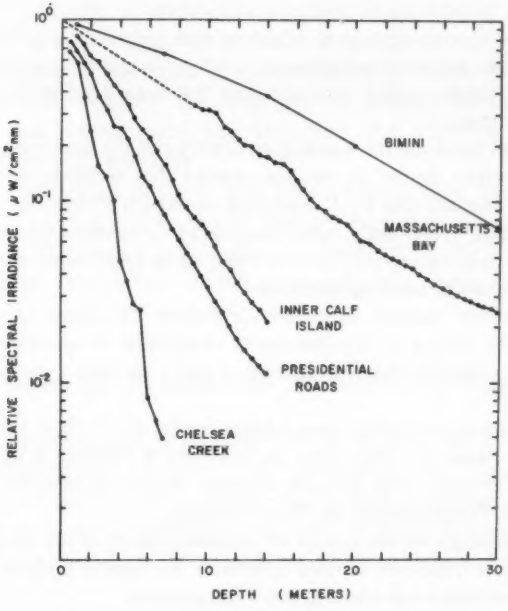

Figure 8 – Irradiance vs depth at 560 nm for 3 locations in Boston Harbor (Aug. 12-24).

The determination of the effects of light variability on the system logically begins with a comprehensive definition of the subsurface light environment. An empirical definition can be established through a systematic study consisting of vertical profiles of spherical spectral irradiance. If the profiles are distributed over a selected geographic range, diversity of water types is assured. The temporal variation must be measured at an appropriate sampling frequency to determine the seasonal, day-to-day and diurnal time constants of the system.

This systematic study can subsequently be used to dictate the selection of light conditions for photosynthetic vs. light condition studies. The intended result is the assignment of relative values to particular sets of light conditions indicative of their effects on photosynthetic rate. These values in turn can be used as the light-photosynthesis interrelationship in productivity estimation techniques.

Radiation Method Cures Adhesives Better

A technique to cure structural adhesives with radiation, a technique which promises to make industrial adhesives more effective and reduce chances of adhesive bonds cracking under thermal stress has been developed at the Naval Research Laboratory.

Conventional methods for bonding structures call for heat-curing of the adhesives. This often results in residual stresses that seriously weaken joints.

Dr. W. D. Bascom and F. J. Campbell of NRL's Chemistry and Nuclear Sciences Division, respectively, who teamed up to develop the new method, said their radiation curing can be very rapid, gives good bond strength and is amenable to industrial bonding operations.

The researchers termed their new technique "a major breakthrough," especially in the joining of graphite-epoxy composites to aluminum, as in aircraft assembly. Residual thermal stresses in joints on such structures are very severe.

The scientists are presently using a linear accelerator (LINAC) to apply electron beam radiation to polyesters. In less than a minute, strong joints are formed. Furthermore, small portable electron sources are available that would allow localized, "spot bonding" by their technique.

This spot bonding would reduce or eliminate much of the complex rigging now necessary to heat-cure bonded structures and would obviate the need to heat entire structures when bonding small components.

A patent is now pending on the NRL development, and work is continuing to optimize the process.

Salt Fingers in the Ocean: A Short History

by Albert J. Williams 3rd

Woods Hole Oceanographic Institution

In 1956, a "perpetual salt fountain" was described in which thermal diffusion through the walls of a pipe would pump cool seawater to the saltier ocean surface. A natural system, salt fingers, operates in the same way on a small scale. Studied in the laboratory since 1960, it has now been found in the ocean. Salt finger convection is one of several mechanisms which can generate oceanic microstructure. A better understanding of the physical and chemical processes associated with microstructure is important to the Navy in order to assess how microstructure, which "creates" small stair-steps in vertical sound velocity profiles, affects the characteristics of high-frequency sound transmission whose acoustic wave lengths are comparable with the size of the stair-steps.

Microstructure, the centimeter scale structure at which molecular diffusion plays a role, is eventually involved in all mixing processes in the ocean. The next larger scale – finestructure – with 1 meter to 100 meter features, has been observed for many years. However, the centimeter scale structure has only been accessible for measurement within the last decade and has attracted the interest of physical oceanographers only recently.

One microstructure process, salt finger convection, was predicted 14 years ago to play a role in the vertical transport of salt and heat in the ocean. It offered a possible explanation of the large vertical eddy diffusion coefficient which is needed for many thermocline models.

Perpetual Salt Fountain and Laboratory Salt Fingers

Stommel, Arons, and Blanchard (1) in a paper in 1956 entitled "An oceanographical curiosity: the perpetual salt fountain" described the convective process since called salt fingering. In the salt fountain, a pipe with thermally conducting walls is suspended vertically in the ocean with its upper end in warm, salty water and its

*Dr. Williams is an Assistant Scientist in the Department of Oceanography at Woods Hole. His main field of interest is microstructure studies.

lower end in denser, cooler, less salty water. The pipe is then primed with water from the lower end. The relatively fresh water in the pipe comes to the same temperature as the outside water at each level. In a simple monotonic gradient, the water in the pipe is everywhere as fresh or fresher than the outside water but at the same temperature as the outside water. This makes the water in the pipe everywhere equally dense or less dense than the outside water so the hydrostatic head in the pipe is less than that outside. The head difference causes water to flow up the pipe which in turn maintains the starting condition that water from the lower end fills the pipe. The perpetual salt fountain is symmetric and will also pump salty water downward if the pipe is first primed with water from the top end.

In the salt fountain process, the pipe provides a mechanism for exchanging heat to eliminate the stabilizing temperature gradient. The salt instability which remains drives the fountain.

In 1960, Stern (2) pointed out that since the molecular diffusivity of heat is one hundred times that of salt, the walls of the pipe are not needed to limit salt diffusion at certain scales. The convective fountain can exist without a pipe. Perturbations of fluid in the form of vertical fingers will grow taller in a gradient region due to preferential diffusion of heat into or out of the finger just as the flow in the pipe is maintained by diffusion of heat across the wall of the pipe.

In the 1960 paper, Stern suggested that this process could be a significant mechanism for the vertical transport of salt and heat in the ocean. No ocean experiments had been performed which allowed an estimate to be made of this importance. But at least one laboratory experiment had been performed by the time of Stern's 1960 paper. Stern included notes by Henry Stommel and Alan Faller of an experiment with dyed, salty, hot water floating on fresh, cold water. Fingers of dye were observed growing down from the interface into the cold water. The size of these fingers agreed closely with a scale which Stern had derived from dimensional arguments.

Turner (3) in 1967 conducted extensive laboratory experiments with salt fingers which he generated at an interface between a mixed layer of warm, salty water and a second mixed layer of cooler, fresher water. He recognized that in general, shear would limit the thickness of the fingering region and would concentrate the overall gradient into a thin region of high gradient separating two layers of low gradient which were stirred by the fingering interface. The flux of salt through the interface drives the convection of the fingers and the layers.

Ocean Finestructure

Preliminary salinity and temperature profiles from the eastern Atlantic off the Straits of Gibralter were available to Turner in 1967. The profiles showed layers of warm, salty water overlying cooler, fresher layers. Turner suggested that salt fingers might exist at the interfaces between these layers. He calculated that if fingers were present, the salt excess would drop out of a layer in 10 days. Thus fingering would be a significant factor in mixing the Mediterranean Outflow water (responsible for these gradients) into the underlying Atlantic water.

In 1968, two papers appeared reporting layers in the ocean. Tait and Howe (4) reported layers in the Mediterranean Outflow and Cooper and Stommel (5) reported layers near Bermuda. The structures were similar, composed of thin interfaces which separated mixed layers. The temperature and salinity decreased with depth. It was suggested that both these cases might be associated with salt fingers which would imply that salt fingering might be very widespread.

The system of layers and interfaces observed in the ocean was related to tank experiments by Stern and Turner (6) reported in 1969. The use of sugar and salt as the two diffusing substances in place of salt and heat allowed them to construct more complicated gradients of each substance. The growth of two fingering interfaces with a convecting layer between them was demonstrated in these experiments. Thus a superficial resemblance to the oceanic data was obtained. Stern and Turner were able to derive the dependence of salt flux across an interface, the thickness of the interface, and the thickness of the convecting layers adjacent to the interface as a function of the salinity difference across the interface. However, the constants of proportionality were unknown functions of the molecular constants determined in these experiments for the sugar-salt system.

Ocean Observation of Salt Fingers

Optical expreiments with sugar-salt fingers reported in 1970 by Shirtcliffe and Turner (7), which revealed the cells to be square-packed in plan view, exploited the refractive index variations within the fingers to produce an image. Stern (8) also reported a technique, in 1970, for measuring salt fingers which relied on optical inhomogeneities of the fingering region. In Stern's analysis, fingers were identified by the refraction of light rays passing horizontally through them. The fingers are vertical, and the refraction is horizontal so that a vertical grid viewed through fingers is distorted while a horizontal grid is not.

I became interested in the detection of salt fingers in the ocean after conversations in the summer of 1969 with Turner and Stommel. Having experimented with Stern's technique and with the schlieren technique used by Turner called shadowgraph, I concluded that shadowgraph was as sensitive as the other and far simpler to use in the ocean.

Following the advice of Stern (8), the sea going version of my shadowgraph contained an instrument to measure salinity and temperature. The complete instrument was untethered to isolate it from cable transmitted ship motion or horizontal drag. Figure 1 is a sketch of the instrument in the ocean. The instrument is called SCIMP for Self-Contained Imaging Micro-Profiler. It sinks slowly, photographing and digitally recording as it goes. The photographs are 16 mm

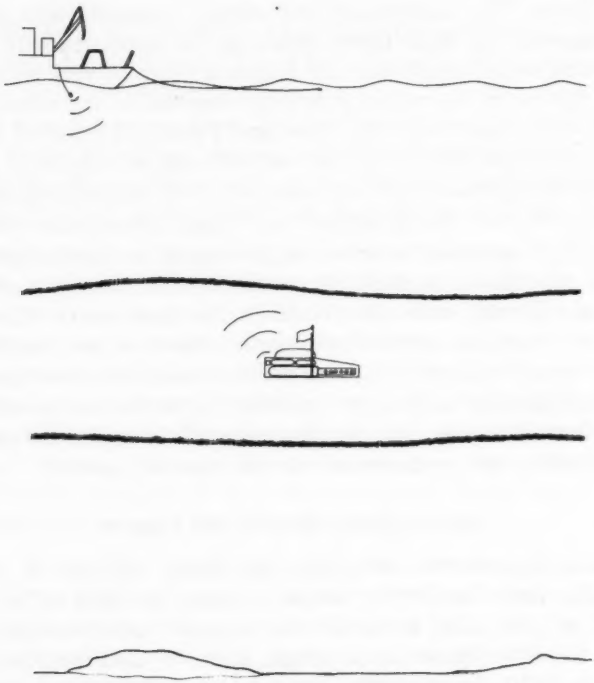

Figure 1 – An autonomous vehicle, a conductivity-temperature-depth microprofiler, and an optical imaging instrument combined as SCIMP (Self-Contained Imaging Micro-Profiler) sinks slowly through microstructure features in the ocean. It is in acoustic communication with a surface vessel.

movies taken at 1 frame per second, of a screen inside the instrument. The shadowgraphs on the screen are produced by a 5 cm diameter laser beam which is reflected through a horizontal path, 160 cm long, in front of the pressure housing. Figure 2 depicts the observation of a fingering interface. Optical inhomogeneities in this seawater path are imaged on the screen. Turbulent structures and fingers have been observed as illustrated in Figure 3.

The instrument was successfully tested in the Caribbean in September, 1972; and in July, 1973, salt fingers were photographed at 1250 meters in the Mediterranean Outflow (9). The fingers occurred

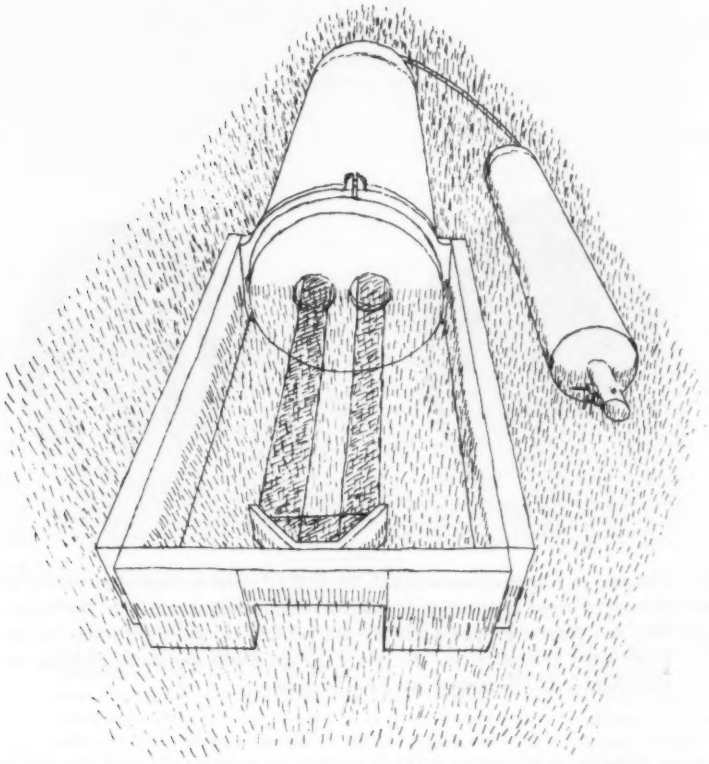

Figure 2 – The optical instrument and the CTD simultaneously measure an undisturbed microstructure feature, here a salt finger interface. The 5 cm diameter laser beam traverses 160 cm of seawater. Refraction by optical inhomogeneities along the path produces a shadowgraph which is photographed within the housing. The CTD measures salinity to .001 $^{o}/_{oo}$, temperature to .0005^{o}C, and depth to 5 cm.

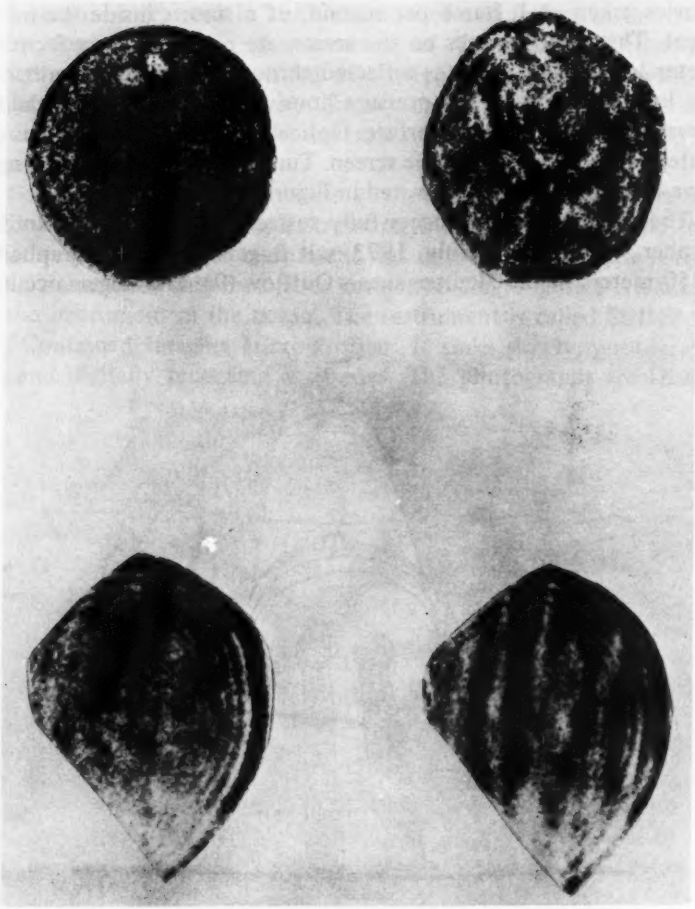

Figure 3 – Shadowgraphs taken by SCIMP show turbulent structure at the upper right contrasted to nearby homogeneous water at the upper left. Salt fingers are indicated by the vertical bands in the image at the lower right contrasted to the image 25 cm shallower without bands at the lower left. The images are 5 cm in diameter.

at an interface between mixed layers, as expected, and the diameter of the fingers was in good agreement with theory. The appearance of the fingers was similar to the laboratory shadowgraphs but the diameters were about twice as great, in agreement with theory. Thus 17 years has brought salt fingers from an oceanographical curiosity to an observed ocean process.

U.S. GOVERNMENT PRINTING OFFICE : 1974 O - 562-391

References

1. H. Stommel, A. B. Arons, and D. Blanchard "An Oceanographical Curiosity; the Perpetual Salt Fountain" *Deep-Sea Research,* 152-153 (1956).
2. Melvin D. Stern "The 'Salt-Fountain' and Thermohaline Convection" *Tellus,* 12 172-175 (1960).
3. J. S. Turner "Salt-Fingers across a Density Interface" *Deep-Sea Research,* 14 599-611 (1967).
4. R. I. Tait and M. R. Howe "Some Observations of Thermo-haline Stratification in the Deep Ocean" *Deep-Sea Research,* 15 275-280 (1968).
5. John W. Cooper and Henry Stommel "Regularly Spaced Steps in the Main Thermocline near Bermuda" *Journal of Geophysical Research,* 73 5849-54 (1968).
6. M. E. Stern and J. Stewart Turner "Salt Fingers and Convecting Layers" *Deep-Sea Research,* 16 497-511 (1969).
7. T. G. L. Shirtcliffe and J. S. Turner "Observations of the Cell Structure of Salt Fingers" *Journal of Fluid Mechanics,* 41 707-719 (1970).
8. Melvin E. Stern "Optical Measurement of Salt Fingers" *Tellus,* 22 76-81 (1970).
9. Albert J. Williams 3rd "Salt Fingers Observed in the Mediterranean Outflow" *Science,* (1974).

NAVAL RESEARCH REVIEWS publishes highlights of research conducted by Navy laboratories and contractors and describes important Naval experimental facilities. Manuscripts submitted for publication, correspondence concerning prospective articles, and changes of address, should be directed to Code 109, Office of Naval Research, Arlington, Va. 22217. Requests for subscriptions should be directed to the Superintendent of Documents, U.S. Government Printing Office, Washington, D.C., 20402. Subscription price: $4.50 per year in the U.S. and Canada; $5.65 per year, foreign; $0.45 per individual copy. The issuance of this periodical approved in accordance with Dept. of the Navy publications and printing regulations.

Editor: WILLIAM J. LESCURE NAVSO P-510

Associate Editors:

A. R. LAUFER, ONR PASADENA

A. R. DAWE, ONR CHICAGO

A. L. POWELL, ONR BOSTON

D. A. PATTERSON, NAVAL RESEARCH LABORATORY

IN THIS ISSUE

VOL. XXVII, NO. 10

Grinding Damage in Ceramics ..... B. G. KOEPKE, R. J. STOKES 1

It is important to understand the defects caused by grinding damage on ceramics in order to learn corrective measures so that ceramics can achieve their full potential in components, devices, and systems.

A Subsurface Light Data Sphere for Irradiance Measurements ..... C. NEEFUS AND G. C. MCLEOD 18

The measurement of irradiance in the upper layers of the ocean is important in evaluating the photosynthetic activity of phytoplankton. Such information is important for communication and detection systems.

Salt Fingers in the Ocean: A Short History ..... ALBERT J. WILLIAMS 27

Marine microstructures, such as salt fingers, affect high frequency sound transmissions in the ocean.

Cover Caption

The effect of substrate surface preparation on magnetic domain configuration in an epitaxial garnet layer. *See page 14.*

DEPARTMENT OF THE NAVY
OFFICE OF NAVAL RESEARCH
ARLINGTON, VA. 22217

OFFICIAL BUSINESS

PENALTY FOR PRIVATE USE, $300.

POSTAGE AND FEES PAID
DEPARTMENT OF THE NAVY
DoD-316

U.S.MAIL

RESRV510ZC FEDLP7208826

JOHN CRERAR
35 WEST 33RD STREET
CHICAGO IL 60616

##